HHS Public Access

Author manuscript

J Immunol. Author manuscript; available in PMC 2024 August 15.

Published in final edited form as:

J Immunol. 2023 August 15; 211(4): 648–657. doi:10.4049/jimmunol.2200703.

The polyanionic drug suramin neutralizes histones and prevents endotheliopathy

Nuria Villalba[1], **Adrian M. Sackheim**[1], **Michael A. Lawson**[1], **Laurel Haines**[1], **Yen-Lin Chen**[2], **Swapnil K. Sonkusare**[2], **Yong-Tao Ma**[3], **Jianing Li**[3], **Dev Majumdar**[1,4], **Beth A. Bouchard**[5], **Jonathan E. Boyson**[1], **Matthew E. Poynter**[6], **Mark T. Nelson**[7,8], **Kalev Freeman**[1,7]

[1]Department of Emergency Medicine, University of Vermont, Burlington, VT USA

[2]Department of Molecular Physiology and Biological Physics, University of Virginia, Charlottesville, VA USA

[3]Department of Chemistry, University of Vermont, Burlington, VT USA

[4]Department of Microbiology and Molecular Genetics, University of Vermont, Burlington, VT USA

[5]Department of Biochemistry, University of Vermont, Burlington, VT USA

[6]Department of Medicine, University of Vermont, Burlington, VT USA

[7]Department of Pharmacology, University of Vermont, Burlington, VT USA

[8]Division of Cardiovascular Sciences, University of Manchester, Manchester, UK

Abstract

Drugs are needed to protect against the neutrophil-derived histones responsible for endothelial injury in acute inflammatory conditions such as trauma and sepsis. Heparin and other polyanions can neutralize histones but challenges with dosing or side effects such as bleeding limit clinical application. Here, we demonstrate that suramin—a widely available polyanionic drug—completely neutralizes the toxic effects of individual histones, but not citrullinated histones (citH3) from NETs. The sulfate groups on suramin form stable electrostatic interactions with hydrogen bonds in the histone octamer with a dissociation constant of 250 nM. In cultured endothelial cells (Ea.Hy926), histone-induced thrombin generation was significantly decreased by suramin. In isolated murine blood vessels, suramin abolished aberrant endothelial cell calcium signals and rescued impaired endothelial-dependent vasodilation caused by histones. Suramin significantly decreased pulmonary endothelial cell ICAM-1 expression and neutrophil recruitment caused by infusion of sub-lethal doses of histones *in vivo*. Suramin also prevented histone-induced lung endothelial cell cytotoxicity in vitro and lung edema, intra-alveolar hemorrhage and mortality

Corresponding author: Kalev Freeman, M.D., Ph.D., 149 Beaumont Avenue, Firestone Medical Research Building 452, The University of Vermont, Burlington, VT, 05405 U.S.A., kalev.freeman@med.uvm.edu; Phone: 802-656-4216.

Author Contributions

NV, AMS, SS, JL, BAB, JEB, MEP, MTN, and KF designed research; NV, AMS, MAL, LH, YLC, SS, and YTM performed research; NV, AMS, MAL, SS, JL, DM, BAB, JEB, MEP, MTN, and KF analyzed data; NV, AMS, and KF drafted the paper. All authors contributed to edits and revisions of the final manuscript.

N.V. current address is Department of Molecular Pharmacology & Physiology, University of South Florida, Tampa, FL, USA. L.H. current address is Department of Microbiology, Immunology & Pathology, Colorado State University, Fort Collins, CO, USA.

Competing Interest Statement: The authors declare no conflicts of interest.

in mice receiving a lethal dose of histones. Protection of vascular endothelial function from histone-induced damage is a novel mechanism of action for suramin with therapeutic implications for conditions characterized by elevated histone levels.

Keywords

endothelium; coagulopathy; histones; polyanion; suramin

Introduction

Acute endotheliopathy is a clinical syndrome resulting from extensive tissue injury in trauma and sepsis, including that attributable to SARS-CoV-2 infection. Endotheliopathy is characterized by widespread disruption of endothelial-dependent vasodilatory function, barrier integrity, and hemostasis which all contributes to thromboinflammation, organ failure, and mortality (1, 2). Extracellular histones are major mediators of endotheliopathy, as shown by the efficacy of anti-histone antibodies in preventing systemic inflammation and mortality in animal models of sepsis and endotoxemia through lipopolysaccharide (LPS) infusion (3, 4). Histones enter the circulation when released by cellular apoptosis or necrosis (5–7), and in innate immunity, when activation of neutrophils leads to the release of chromatin in the form of neutrophil extracellular traps (NETs). These NETs contain granular enzymes and peptides which aid in clearing bacteria, and nuclear proteins, predominately histones (3, 4). Nucleosomes induce cytokine production at low concentrations, but high concentrations kill cells (8). Evidence of NET-induced endothelial damage has been reported in COVID-19 (9), atherosclerosis (10, 11), ischemia/reperfusion (12), and venous thrombosis (13, 14). Plasma nucleases act on DNA-histone complexes circulating in the blood to degrade the nucleic acids, exposing the highly cationic histones that function as damage-associated molecular pattern proteins, activating the immune system and causing additional toxicity (15–17). Free histones are found at low levels (2–5 μg/mL) in the circulation in uninjured humans, but levels can reach 20–100 μg/mL in COVID-19 patients (18) and up to 250 μg/mL in the acute period following severe trauma before they are degraded over hours and days by the protease activated protein C (19). At high concentrations, histones can activate platelets and damage vascular cells, particularly pulmonary (19) and mesenteric endothelial cells (20), vascular smooth muscle cells (11) and erythrocytes (21, 22), but histones are not directly toxic to endothelial cells in the cerebral vasculature (23). Histones activate and injure endothelial cells through mechanisms including calcium overload (3, 20), pyroptosis through NLRP3 inflammasome and toll-like receptor activation (TLR) (6, 24–27), and disassembly of adherens junctions causing loss of barrier function (23, 28). Histones, like other cations can also bind directly to anionic membrane phospholipids in stoichiometric ratios (29, 30), with high concentrations leading to disruption of lipid bilayers (11, 31). Furthermore, histones deposited on the lumen of blood vessels can also attract monocytes in a surface-charge dependent fashion causing atherosclerosis (4). Elevated histone levels have been linked to widespread endothelial injury and organ damage in human patients after trauma (19, 32–38) and other conditions including ischemic stroke (39), sepsis (3), pancreatitis (40), and acute respiratory distress syndrome (ARDS) (41, 42).

The critical unmet need for therapeutics that protect the vascular endothelium from histone-mediated injury has become of immediate relevance in the context of the SARS-CoV-2 pandemic (1, 9, 43). It was recently demonstrated that the polyanionic agent defibrotide can neutralize the pathological effects of extracellular histones (44). This is important, because it suggests a strategy to protect blood vessels from the products of NETosis. However, defibrotide is an expensive drug that typically requires dosing every 6 hours. Other synthetic polyanions can also block histone-induced toxicity (22), but these have not yet been FDA-approved for human use. We hypothesized that suramin - a polyanionic drug, which is also safe, inexpensive, and widely available - would effectively prevent histone-induced endotheliopathy. First synthesized by Bayer in 1917 as part of a drug discovery program for trypanosomiasis (African sleeping sickness), suramin is a bis-polysulfonated naphthylurea hexaanion with activity against trypanosomes in both animal models and humans (45). Suramin has been used clinically for over 100 years and, importantly, is considered among the safest and most effective drugs for health care by the World Health Organization. Unlike heparan sulfate or heparin synthetic polyanions, which also bind histones, suramin dosing is infrequent (usually once per week), well-tolerated, and does not cause complications associated with anticoagulation.

The objective of this study was to test the hypothesis that suramin can protect against histone-induced endothelial dysfunction. We found that suramin binds individual histones in solution, but not citrullinated histones released from NETs, which is consistent with the lack of protection against citH3-induced cytotoxicity. Histones activated cultured human endothelial cells to promote rapid thrombin generation; we found that this reaction is abolished by suramin. In pressurized murine vascular preparations, we directly tested the efficacy of suramin for preventing histone-induced aberrant endothelial calcium signaling and vasodilatory dysfunction. In a histone infusion model, we measured the extent to which suramin prevented histone-induced lung injury, endothelial cell activation, adhesion molecule expression, and pulmonary barrier disruption. Importantly, we also found that suramin completely protects against lethal doses of histones. Thus, histone binding is a novel mechanism of action for suramin, and these experiments provide support for the use of suramin as a strategy to protect against histone-induced endotheliopathy.

Materials and Methods

Animals.

Male C57BL/6 J mice (12 weeks old; ~30 g) were purchased from The Jackson Laboratory (Bar Harbor, ME). All animals were maintained on 12-hour light/dark cycle and standard diet and water *ad libitum* in an AALAC-accredited facility. All animal experiments were approved by the University of Vermont's Institutional Animal Care and Use Committee (IACUC 2020–000-175), in accordance with the recommendations in the Guide for the Care and Use of Laboratory Animals of the National Institutes of Health, and efforts were made to minimize suffering.

In vivo histone exposure.

Mice were anesthetized with 2.5% isoflurane and administered purified histones (Roche® distributed by Sigma-Millipore; #10223565001) or sterile saline (control group) as a single dose via retroorbital sinus. Histones were diluted in sterile saline to yield doses of either 45 mg/Kg or 75 mg/Kg.

Suramin trial *in vivo*.

We conducted a preclinical randomized trial to establish efficacy of suramin in histone exposure. Based on the recommended initial dose of suramin (1 g for adults and 10–15 mg/Kg for children) (http://home.intekom.com/pharm/bayer/suramin.html), we used 20 mg/Kg as the human reference dose. We planned to compare n=10 animals each in control (histone alone) and suramin (20 mg/Kg) groups based on sample size estimations for survival analysis in a two arm trial. For dose finding, we also included an additional arm o with higher dose of suramin (n=6, 50mg/kg). The fourth arm of the study was a control group that did not receive histones or suramin to establish baseline (n=6). Mice were randomly assigned to the 4 treatment groups. Suramin (Adipogen; #AG-CR1–3575) was administered intraperitoneally (20 mg/Kg; 50 mg/Kg) 1 hour prior to histone infusion in the suramin groups. Animals were then anesthetized to received either histones or controls. The primary outcome was the effect of suramin on survival in the face of a lethal dose of histones (75 mg/kg; intravenously) (1). Survival rates were determined every five minutes for 1 hour.

Secondary outcomes of inflammatory biomarkers, lung inflammation (histology of lavage fluid and parenchyma), pulmonary endothelial cell activation, and pulmonary vascular permeability, were studied to provide additional insight into suramin's mechanism of action in vivo. These outcomes were assessed in additional experiments utilizing a survivable dose of histones (45 mg/kg; intravenously) in mice, randomized to receive either no treatment (histones alone) or suramin (50 mg/kg). Additional controls were included that did not receive histones or suramin to establish baseline for each outcome. All mice were terminally anesthetized and euthanized 24 hours after treatment.

To assess for markers of inflammation relevant to activated endothelium, blood was collected via cardiac puncture in BD Microtainer® blood collection tubes (BD Biosciences). Sera was obtained by centrifugation (1,300 x g, 10 min) and frozen. Thawed sera were diluted two-fold and cardiovascular markers were measured using a Milliplex mouse cardiovascular disease magnetic bead panel (Millipore-Sigma; #MCVD1MAG-77K). Data were acquired using the Bio-Plex suspension array system and Bio-Plex Manager software.

To assess inflammation in the lung, bronchoalveolar lavage (BAL) fluid was collected and analyzed for total number of leukocytes and total protein. Euthanized mice were tracheotomized with an 18-gauge cannula and lavaged with 1 mL Dulbecco's phosphate-buffered saline (Life Technologies, Carlsbad, CA). Lavage fluid was centrifuged (1,300 x g, 10 min) and cell-free supernatants were snap-frozen for total protein analysis using the Pierce™ BCA protein assay kit (Thermo Scientific; #23227). The pellet was resuspended with 400 μL of PBS and total leukocyte count was measured via a hemocytometer (Neubauer chamber).

Intact lungs were also assessed for histological changes. Lungs were inflation-fixed at 20 cm H_2O pressure with buffered formalin for 24 hours, embedded in paraffin, sectioned, and stained with hematoxylin and eosin.

Pulmonary endothelial cell activation was studied in isolated cells by flow cytometry. Mice were euthanized using sodium pentobarbital. Lungs were inflated with an enzymatic digestion buffer (Dubecco's modified Eagle's medium [DMEM], 1 mg/mL collagenase type IV [Invitrogen], and 0.2 mg/mL DNase I [Sigma]), after which they were dissected away from the trachea and heart and incubated in 5 mL enzymatic digestion buffer in a 50 mL conical tube for 30 min at 37°C under agitation at 200 rpm. After the 30-min incubation, 25 mL of PBS was added, and the samples were vortexed for 30 seconds. The resulting cell suspension was passed through a 70-μm filter and washed in PBS. Red blood cells were lysed using Gey's solution and washed in PBS–2% fetal calf serum, after which cells were counted and resuspended for flow cytometry experiments.

For flow cytometry, nonspecific antibody binding was blocked by incubating 1×10^6 cells with FcBlock anti-CD16/32 (BD Biosciences; #553141). After washing, cells were stained at 4°C in PBS–2% FCS containing 0.1% sodium azide. Reagents and antibodies used in these experiments were as follows: Live/Dead™ (1:500; Invitrogen; #L23105), CD45-FITC (1:400; eBioscience; #MCD4501), CD11c-PECy7 (1:200; BD Biosciences; clone HL3 #561022), CD11b-eFluor450 (1:800; eBioscience; cone M1/70 #48–0112-82), Ly6G-Alexa Fluor700 (1:500; BD Biosciences; clone 1A8 #561236), CD45-BB700 (1:6400; BD Biosciences; #566440), CD326-BV605 (1:500; BD Biosciences; #740389), CD31-FITC (1:400; BD Biosciences; #558738), CD141-BV421 (1:800; BD Biosciences; #747647). Data were collected on a BD LSRII flow cytometer (BD Biosciences) and analyzed using FlowJo (TreeStar, Ashland, OR). Antibody titration experiments were performed to determine the antibody concentration resulting in the best separation of cell populations and minimize nonspecific binding under same experimental conditions.

Pulmonary vascular barrier permeability to solutes was assessed by measuring extravasation of FITC-labelled 70-kDa dextran. For these studies, mice were re-anesthetized 24 hours after experimental treatment, and then given a retroorbital injection of 70-kDa FITC-dextran (100 μL of 3 mg/mL). After 30 minutes, they were euthanized with transcardial perfusion with PBS to eliminate any remaining FITC-dextran in circulation. Lungs were isolated and homogenized in 1 mL RIPA buffer and centrifuged at 12,000 x g for 20 minutes. The concentration of 70-kDa FITC-dextran in the supernatant was detected via fluorescence measurement (excitation 490 nm, emission 520) and interpolation from a standard curve of known concentrations of FITC-dextran. Results are presented as ng of FITC-dextran per mg of protein in the supernatant.

Calcium imaging in pulmonary arteries *ex vivo*.

Calcium imaging in the native endothelium of mouse pulmonary arteries was performed as previously described (46). Briefly, 4th-order (~50 μm) pulmonary arteries were pinned down *en face* on a Sylgard block and loaded with Fluo-4-AM (10 μM) in the presence of pluronic acid (0.04 %) at 30° C for 30 minutes. Fluo-4 was excited at 488 nm with a solid-state laser and emitted fluorescence was captured using a 525/36-nm band-pass filter.

Images were acquired at 30 frames per second with Andor Revolution WD (with Borealis) spinning-disk confocal imaging system (Oxford Instruments, Abingdon, UK) comprised of an upright Nikon microscope with a 60X water dipping objective (numerical aperture 1.0) and an electron multiplying charge coupled device camera (iXon 888, Oxford Instruments, Abingdon, UK). Ca^{2+} signals were analyzed using the custom-designed SparkAn software (46, 47). A region of interest defined by a 1.7-μm^2 (5×5 pixels) box was placed at a point corresponding to peak event amplitude to generate a fractional fluorescence (F/F_0) trace. F/F_0 traces were filtered using a Gaussian filter and a cutoff corner frequency of 4 Hz. The number of Ca^{2+} events was auto-detected using a detection threshold of 0.3 F/F_0 in SparkAn (custom software, Dr. Adrian Bonev, Burlington, VT). Each data point indicates one field of view from one pulmonary artery. Calf thymus histones containing H1, H2a, H3, H4 histones (unfractionated histones) were used for these experimental series.

Histone-mediated cytotoxicity assay in cultured cells.

The cytotoxicity of calf-thymus histones and citrullinated histones H3 was determined on mouse lung microvascular endothelial cells (Cell Biologics; #C57–6011) using propidium iodide (PI). Cells were treated with various concentrations of histones or citrullinated Histone H3 and then incubated with PI (2 μg/mL) for 20 min at 37 °C. Then, PI fluorescence was quantified using a microplate reader and dead cells were visualized under a confocal microscope.

Calibrated automated thrombinography in cultured cells.

Human endothelial cells (EA.hy926; ATCC® CRL-2922™) were incubated with histones (50 μg/mL), suramin (50 μM), histones + suramin, or Dulbecco's Modified Eagle Medium alone for 4 hr at 37°C, 5% CO_2. Calf thymus histones containing H1, H2a, H3, H4 histones (unfractionated histones) were used for these experimental series. The cells were released from the tissue culture wells with trypsin and subjected to centrifugation (170 x g, 7 min). Cell pellets were washed one time by resuspension in 20 mM HEPES, 0.15 M NaCl (pH 7.4) (HBS) followed by centrifugation. The final cell pellets were resuspended in HBS and adjusted to a final concentration of 1×10^7/mL.

Thrombin generation was assessed using a modified calibrated automated thrombogram. Plasma was thawed at 37°C in the presence of corn trypsin inhibitor (0.1 mg/mL final concentration) and incubated with the thrombin substrate Z-Gly-Gly-Arg 7-amido-4-methylcoumarin hydrochloride (0.42 mM) (Bachem AG, Switzerland) and $CaCl_2$ (15 mM) (3 min, 37°C). The reactions were initiated by the addition of relipidated tissue $factor_{1–242}$ (6.5 pM) (a gift from Dr. R. Lunblad, Baxter Healthcare Corp.) and synthetic vesicles consisting of 80% phosphatidylcholine and 20% phosphatidylserine (PCPS) (20 μM), or EA.hy926 cells (2×10^5). Fluorescence was measured (ex = 370 nm/em = 460 nm) for 1 hour with a Cytation 3 imaging reader (BioTek, Winooski, VT). Changes in fluorescence were converted to thrombin concentrations using a calibration curve created from sequential dilutions of human thrombin. If no change in fluorescence was noted after 60 min, the lag time for the sample was defined as >60 min.

Fluorescence spectroscopy.

Fluorescence spectroscopy was used to determine the equilibrium dissociation constant (K_d) values for the histone-suramin complex. Calf thymus histones containing H1, H2a, H3, H4 histones (unfractionated histones) or citrullinated histone H3 (Cayman chemicals; #17926) were used for binding experiments. The changes in intrinsic suramin fluorescence emission were measured with a microplate reader (BioTek; Winooski, VT) at 25 °C. The samples were excited at 315 nm and the emission spectrum was measured between 370–480 nm. Histones did not show spectral overlap in that range (Supplemental Fig. 1 A). The titration was performed stepwise with a suramin stock concentration (1 μM) in assay buffer containing 50 mM HEPES, 100 mM NaCl and 2 mM $CaCl_2$ (pH 7.4); fluorescent measurements were performed after each titration with histones (0 to 8 μM). After normalization of the fluorescence emission signal, K_d for each suramin-histones complex was estimated by nonlinear curve fitting with a sigmoidal dose–response function using GraphPad 7 software (GraphPad, San Diego, CA). The percentage of bound suramin-histones was plotted against the concentration of free histones.

Molecular modeling.

Model Preparation.—All the models were constructed using the Desmond/Maestro program (v2016–3 Schrödinger, Inc.) using the System Builder in Maestro. Each model contained a complete histone octamer (PDB: 5XF3) with or without DNA and six suramin molecules that were arbitrarily placed at a minimum distance of 15 Å from the proteins. The SPC water model was employed to solvate the complexes, with counter ions and 0.12 M NaCl, 0.047 M KCl, 0.025 M $CaCl_2$, and 0.012 M $MgCl_2$. The construct with a DNA-bound histone has a total of 197,122 atoms in a periodic box of ~123×128×127 $Å^3$, while the one with a DNA-free histone has 180,860 atoms in a box of ~ 120×122×124 $Å^3$.

Simulation setup.—All simulations were performed in the Desmond program with the OPLS3 force field in the NPT ensemble (1.01325 bar, 310 K, Martyna-Tobias-Klein coupling scheme) with a time step of 2 fs(48, 49). The particle mesh Ewald technique was used for the electrostatic calculations. The Van der Waals and short-range electrostatics were cut off at 9.0 Å. Hydrogen atoms were constrained using the SHAKE algorithm. Each simulation has two 700-ns replicas.

Visualization and Analysis.—PyMOL (v2.5, Schrödinger, Inc.) and Visual Molecular Dynamics (VMD, http://www.ks.uiuc.edu/Research/vmd/) were used for the structure visualization of the simulations; the simulation analysis panel was carried out in Maestro.

Statistics.

Data sets were first tested for normal distribution using the Kolmogorov-Smirnov method to determine the appropriate parametric or non-parametric test with which to proceed. Data were analyzed by two-tailed unpaired or paired Student’s T-test, Mann-Whitney U-test, Wilcoxon rank text, one-way or two-way ANOVA and Bonferroni post-hoc test, or the Mantel-Cox test for survival, using GraphPad Prism 7.04 (GraphPad Software, Inc, La Jolla, CA). A P value less than 0.05 was considered statistically significant.

Results

Suramin binds to individual histones in solution and decreases histone-mediated cytotoxicity.

Based on its molecular structure, we hypothesized that suramin, a highly charged polysulfonated napthylurea, would bind avidly to cationic histone complexes (Fig. 1 A). When NETs or nucleosomes enter the bloodstream, they are exposed to endogenous nucleases that rapidly digest DNA, leaving free histone proteins (15). Therefore, we focused on testing the interactions between suramin and histones. First, fluorescent spectroscopy studies were used to biochemically establish the dissociation constant (K_d) and number of high-affinity binding sites for interactions between the two molecules. We established the absorbance and emission spectra for histones and suramin in solution, and then measured suramin sodium salt intrinsic fluorescence using an excess of suramin in the presence of increasing concentrations of histones (Fig. 1 B; Supplemental Fig. 1). The resulting interactions are represented using a binding curve (Fig. 1 C). Scatchard analysis of the binding curve demonstrates a single high-affinity binding site with a dissociation constant (K_d) of 250 nM (Fig. 1 C). These results confirm that suramin readily binds histones in solution. We then used all-atom molecular dynamics (MD) simulations to determine likely interactions between suramin molecules and the histone octamer in solution (Fig. 1 D and Supplemental Video 1). Suramin quickly formed electrostatic contacts between its SO_3^- and arginines (Arg) on the protein surface such as Arg53 and Arg69 of H3, Arg23 and Arg45 in H4, Arg17 in H2A and Arg30 in H2B. Hydrogen bonding between suramin and several threonines (Thr) was also observed, such as Thr80 of H3, Thr16 and Thr76 in H2A, and Thr116 in H2B. These interactions remained stable toward the end of our simulations and enabled steady binding for five of the suramin molecules to histones. Additionally, we tested the interaction between citrullinated H3 and suramin. Binding experiments by fluorescence spectroscopy revealed no changes of the citrullinated H3 fluorescence peak in the presence of suramin, indicating a lack of binding (Supplemental Fig. 2 A). We next studied whether suramin affects cytotoxicity induced by either individual histones or citrullinated H3 by PI staining. Suramin significantly decreased cell death induced by 100 ug/mL histones, while treatment with suramin did not protect against citrullinated H3 (Supplemental Fig. 2 B and C). These results further suggest that suramin binds to individual histones preventing endothelial cell cytotoxicity but does not bind as effectively to NET-derived histones.

Histones induce rapid thrombin generation on human endothelial cells that is blocked by suramin.

Thrombin is the ultimate protease in the clotting cascade, catalyzing fibrin formation. The formation of thrombin following cleavage of prothrombin is the rate limiting to the coagulation process (50). Phosphatidylserine-dependent prothrombin activation on the endothelial surface leads to the formation of microthrombi, shedding of extracellular vesicles and glycocalyx, neutrophil migration, and efflux of water into damaged interstitial tissues (10, 50). Extracellular vesicles, enriched with histones, have procoagulant membranes and carry microRNAs into the bloodstream (51). To test whether histones promote thrombin generation, we used calibrated automated thrombograms in recalcified pooled healthy human plasma, in the absence of exogenous tissue factor and phospholipid

membrane, to measure the ability of cultured human endothelial cells (Ea.hy926) to support thrombin production. Under these conditions, thrombin formation occurred slowly (lag time >15 minutes), but when histones were applied, thrombin generation was accelerated, with a lag time of <5 minutes (Fig. 2 A and B). Histone treatment also had prothrombotic effects on other measures of thrombin generation including peak thrombin, endogenous thrombin potential, time to peak thrombin, and the rate of thrombin generation (Fig. 2 C–F). In the presence of suramin, measures of histone-induced thrombin generation were significantly ameliorated to levels observed in untreated cells.

Suramin prevents disruption of endothelial-dependent vasodilation and endothelial cell calcium overload caused by histones.

Endothelial-dependent vasodilation of small arteries in response to nitric oxide and other hyperpolarizing stimuli is essential for the regulation of regional blood flow to meet metabolic demands. Disruption of endothelial-dependent vasodilation is considered the hallmark of endothelial dysfunction. We previously demonstrated that histones induce aberrant endothelial cell calcium responses that disrupt normal vasodilatory signals in small mesenteric arteries (10, 47). Here, we used video-edge detection to record the vasodilatory responses of pressurized, resistance-sized arteries from the mouse mesenteric circulation to the exposure of the endothelial-dependent vasodilator NS309 (0.1 μM to 1 μM) before and after intraluminally perfusing histones (10 μg/mL) through the vessel in the presence and absence of suramin (50 μM) (Fig. 3 A and B). Vasodilation to 1 μM NS309 after 30 minutes of histone exposure was reduced to 33 % of the pre-histone control dilation. Vasodilatory function was completely preserved during this same experiment while in the presence of suramin (50 μM). Because lung injury is a significant concern in conditions characterized by high levels of histones such as ARDS (19), we also studied vascular preparations from small mouse pulmonary arteries. These blood vessels were surgically opened on one side to expose the endothelial cell layer for direct measurement of a fluorescent calcium indicator using confocal microscopy (Fig. 3 C and D). Similar to our prior findings in human and mouse mesenteric arteries (20), we found that histones (10 μg/mL) significantly increased the number of detectable calcium events compared to baseline. The presence of suramin (50 μM) during histone application significantly decreased the number of calcium events; however, the activity was still elevated when compared to the baseline control (Fig. 3 D). Together, pre-treatment with suramin completely prevents histone-induced endothelial vasodilatory dysfunction in pressurized arteries and significantly decreases aberrant calcium signaling caused by exposure to histones.

Suramin prevents adhesion molecule expression, neutrophil recruitment, and pulmonary endothelial barrier disruption caused by histones.

The results of our biochemical and *in vitro* work provided a rationale for an *in vivo* model of histone toxicity. Circulating histones can injure platelets, erythrocytes and vascular endothelial cells from multiple tissue beds. However, in humans and animal models of trauma, lung tissue is particularly vulnerable to circulating damage associated molecular pattern proteins (19). Therefore, we next tested the hypothesis that suramin would prevent the increase in circulating biomarkers, endothelial cell activation, and influx of inflammatory cells into the lungs caused by histone infusion (45 mg/Kg). To specifically assess the

endothelial effects of suramin after histone exposure, we freshly isolated mouse pulmonary endothelial cells and measured their adhesion molecules using flow cytometry. The extent of neutrophil migration into the lungs after histone exposure was also quantified. After 24 hours, lung tissue was dissociated, and the frequency of neutrophils determined by expression of CD11b and Ly6G by flow cytometry. Treatment with histones resulted in a statistically significant increase in the frequency of neutrophils in the lung (Supplemental Fig. 3 A and B). Lung endothelial cell Intracellular Adhesion Molecule-1 (ICAM-1) expression was also significantly increased by histones (Supplemental Fig. 3 C and D). Suramin ameliorated these histone-induced effects, causing a significant reduction in the frequency of neutrophils and expression of endothelial cell ICAM-1.

Suramin prevents lung injury and improves survival after exposure to histones.

To assess clinically relevant outcomes, we next tested whether suramin would prevent death and lung injury *in vivo* after histone exposure. We randomized mice to one of 4 experimental groups: saline; saline and histones (75 mg/Kg); suramin (20 mg/Kg) and histones; or suramin (50 mg/Kg) and histones (Fig. 4 A). Survival was monitored and updated every minute for the 35-minute duration of the study. Groups were compared using a Mantel-Cox analysis and Mantel-Haenszel for the Hazard Ratio. Seventy percent (70 %) of animals receiving 75 mg/Kg of histones alone died abruptly within 10 minutes and showed symptoms such as bleeding from the nose, pink frothy sputum and signs of respiratory distress, and only 20 % survived the 35-minute period. In contrast, 100 % of animals receiving suramin at the higher dose of 50 mg/Kg with the lethal dose of histones survived when compared to the histone group (1.959 to 35.09 95 % CI; 8.29 Hazard Ratio; $P<0.05$; *). The lower dose of suramin (20 mg/Kg) also provided a modest survival benefit (36 %) when compared to the high dose (1.359 to 28.71 95 % CI; 6.25 Hazard Ratio; $P<0.05$; *) but not to the histone only group (0.9702 to 9.410 95 % CI; 2.49 Hazard Ratio; n.s.). In a separate set of mice exposed to histone infusion (45 mg/Kg) in the presence or absence of the higher dose of suramin (50 mg/Kg), we found that suramin reversed intra-alveolar hemorrhage visible on histology, and elevation in cell counts and protein measured in broncho-alveolar lavage fluid (Fig. 4 B and C). As an additional control, we also examined lung sections from mice receiving suramin alone (50 mg/Kg). These were indistinguishable from mice treated with saline (Supplemental Fig. 4 A). Pulmonary barrier breakdown induced by histones, quantified as the extravasation of 70-kDa FITC-labeled dextran, was significantly decreased by suramin. Suramin also blocked extravasation of the labeled dextran in renal tissue caused by histones (Supplemental Fig. 4 B).

Discussion

Histones, released from injured cells or in NETs extruded from activated neutrophils, can activate and damage vascular cells through several mechanisms that are not fully understood. Histones can activate ion channels, observed by membrane potential and current recordings in endothelial cells and other cells (19, 52, 53). With prolonged exposure (minutes to hours), or at high concentrations, histones – and histone H4 in particular – can also damage lipid bilayers in any cell type, including endothelial cells, and act as cell-penetrating proteins (11, 22, 31). Histones can also engage innate immune responses leading to prothrombotic

activation of endothelial cells (27, 54, 55) or pyroptosis (6, 24–26). All these mechanisms can contribute to acute endotheliopathy. Here, we looked at the interaction between extracellular histones and suramin and demonstrated that not only does suramin form a stable complex with histone proteins, but also, this neutralizing effect completely prevents histone-induced endothelial dysfunction and mortality. Furthermore, we also explored the interaction between NET-derived histones (i.e. citrullinated histones) and suramin. We found that citrullination, an important post-translational modification on histones essential for the formation of NETs, prevents the interaction between citH3 and suramin. The loss of charge on NET-derived histones most likely decreases the binding force between citrullinated histones and suramin, and therefore suramin's chelating (protecting) effect. Suramin has been used for over 100 years as an anti-parasite and anti-cancer agent, and, importantly, is considered among the safest and most effective drugs for health care by the World health organization. This discovery of a new mechanism of action for a widely available and easily administered drug, as a blocker of deleterious histone effects, provides a tantalizing target for the potential clinical therapeutic use of suramin in acute immuno-vascular and thrombo-inflammatory conditions.

Our results provide new insight into the pathophysiological outcomes of histone-induced organ injury. We provide the first demonstration that in native, pulmonary artery preparations, histones elicit calcium-mediated events like those we previously observed in mesenteric resistance arteries from human and mouse. We also found that histone infusion caused endothelial barrier breakdown of small blood vessels in both kidney and lung, with increased extravasation of the 70-kDa dextran, but not brain. This is consistent with other evidence that pulmonary and renal (6, 17, 19) tissue beds are highly sensitive to histone-induced injury. It was recently shown that histones increased paracellular permeability in the hippocampus but not cortical brain regions (23). It is possible that we missed these regional cerebrovascular effects because we quantified vascular leak for the entire brain and not specific regions, or because we used a 70-kDa tracer rather than a smaller sized dextran which would more specifically target blood-brain barrier permeability. Here, our focus was on lung injury, with results in freshly harvested lung cells, isolated vascular preparations, and *in vivo* models uniformly supporting model in which histones activate endothelial cells to increase cellular adhesion molecule expression, in conjunction with increased release of circulating adhesion molecules. These changes in the pulmonary vascular endothelium result in increased neutrophil recruitment to the lungs.

Importantly, we also demonstrate a new, endothelial-dependent mechanism by which histones increase thrombosis. Prior studies have shown that histones can increase plasma thrombin generation in purified systems by reducing thrombomodulin-dependent protein C activation (56). Here, we provide new evidence that histones can rapidly activate endothelial cells directly to promote thrombin generation. We show that on endothelial cells, in the absence of added tissue factor (TF) or phospholipids, thrombin formation occurs slowly, but when histones are applied, thrombin generation is accelerated, with a lag time of <5 minutes. This reaction was blocked by suramin. The time course of this reaction, occurring minutes after histone exposure, is not consistent with known pro-coagulant responses of endothelial cells to histones, such as release of VWF (54), upregulation of TF (27), or downregulation of thrombomodulin mRNA and surface antigens (55) which occur 1 to 8 hours after exposure.

Thus, rapid phosphatidylserine translocation, possibly due to TMEM16f activation (57, 58), coupled with mobilization of “cryptic” TF in the endothelial cell membrane, likely drive the rapid reactions we observe. Understanding the effectors of rapid procoagulant responses to histones may improve targeted therapies to protect against excessive thrombosis in inflammatory conditions.

Suramin offers several advantages over other therapeutic strategies to prevent histone-medicated vascular injury. Polyanions such as heparin can neutralize histones and prevent histone-mediated cytotoxicity (42, 59–61). Heparin improves outcomes in some patients with sepsis (59) or COVID-19 (62, 63), but the mechanisms are not fully understood. Furthermore, heparin cannot be safely used in all patients, such as those requiring surgical procedures, because of the risk of hemorrhagic bleeding. Unlike heparin which requires continuous infusion, suramin dosing for acute inflammatory conditions is infrequent (once per week), and extensive experience with this drug has shown that it has an excellent safety profile. Anticoagulant effects have been demonstrated in trials of continuous infusions of suramin after 14 days, but single injections of suramin do not impact blood clotting(64). It is also readily available world-wide, at a low cost. Other naturally-occurring substances, such as pentraxin 3 (65), activated protein C (APC) (35), C1 esterase inhibitor (66), and inter-α-inhibitor proteins (39); anti-histone antibodies (3, 4, 42) and synthetic polyanions (22, 44), can also neutralize excessive histones to prevent toxicity, but these drugs are either not approved or not available for human use. Albumin or fresh frozen plasma may have benefits in trauma and sepsis, in part due to histone binding (67), but blood products are limited resources with high costs compared to suramin.

Taken together, these results provide evidence supporting the use of suramin in trauma and sepsis. This is particularly important in the context of the unprecedented global public health crisis caused by the novel SARS-CoV-2 virus, because histone levels are elevated in individuals with COVID-19 (18, 68), and endotheliopathy and thromboinflammation secondary to NETs drives progression from systemic inflammation to organ failure and death (1, 2). Of note, suramin may have other mechanisms of therapeutic action in viral illness. Polyanion inhibitors have been used to block viruses that require cell surface sugars such as heparan sulfate (HS) to infect humans, which include HIV, Ebola, Zika, and SARS. These inhibitors include naturally occurring therapeutic polyanions such as heparin, synthetic polyanions, such as suramin, or modified cyclodextrins (69). Heparin is the subject of over a dozen registered clinical trials for SARS-CoV-2 (clinicaltrials.gov) and has efficacy in COVID-19 (63). Most of these trials are testing injectable unfractionated heparin or low molecular weight heparin at prophylactic or therapeutic anticoagulant doses. Other trials are using intranasal or nebulized heparin in an attempt to block viral entry, because heparin can serve as a decoy for the target cell heparan sulfate needed for optimal interaction between viral spike protein and ACE2. Heparin is also believed to have immunomodulatory and endothelial protective effects, based on evidence of prior benefit in sepsis from other causes, and histone binding may be an important therapeutic mechanism of action for heparin (59, 70). Suramin is a competitive inhibitor of heparin, and it has been suggested – but not established – that suramin shares a mechanism of action against SARS-CoV-2 by acting as a decoy for heparan sulfate that can block spike protein and ACE2 interactions (71). Suramin

also inhibits the main protease needed for SARS-CoV-2 infection (72), and it is the subject of at least one COVID-19 clinical trial at the time of this submission (clinicaltrials.gov).

While our data demonstrate that direct interaction and neutralization of histone proteins is a mechanism of action for suramin, we did not rule out the possibility that the drug has other mechanisms which might contribute to endothelial protection. For example, previous studies have demonstrated mechanisms of action for suramin, including known effects on several many enzymes and receptors. Published studies show that suramin exhibits activity blocking downstream G protein mediated signaling of various GPCR proteins including A1 adenosine receptor, D2 receptor, P2 receptor, rhodopsin and ryanodine receptors(73–76). Suramin was also reported to inhibit human sirtuins (SIRT1/T)(77). Additionally, at high concentrations, suramin has cell-independent effects on blood coagulation and clot formation(64). Whether these mechanisms involved in endothelial cell protection and improved mice survival and/or improved acute lung injury caused by histones was not studied here. Because our study was focused on histone-induced microvascular damage and the protective effect of suramin in this context, we did not include mice receiving suramin alone in all experiments. Although this is a limitation to our work, the literature already contains several studies examining the effects of suramin alone. For example, an experimental group receiving suramin alone at a similar dose (60 mg/Kg) was included in a previous study that examined effects of suramin on the lung in the context of bleomycin induced lung injury (78). The mice receiving suramin had no difference in survival from those receiving saline. Furthermore, suramin alone had no impact on total and differential cell count in BAL fluid. This contrasts with the effects of toxic doses of suramin (250–500 mg/Kg), which produces abnormal enlargement of lungs and evidence of lung pathology like the lysosomal storage disorder, mucopolysaccharidosis (79, 80). Of note, the combination of histone and suramin produced an ICAM-1 response that appears even lower than histones alone (Supplemental Fig. 3 D). This suggested that the protective effects of suramin in the context of histone exposure may be explained not only by binding histones in solution, but also through other mechanisms of action. In support of this, prior work has shown that suramin alone can decrease immunogenicity of renal endothelial cells by reduction in their expression of ICAM-1 (81). In another study, suramin suppressed cell membrane permeability in cultured kidney cells via inhibitory actions on connexin 43 hemichannels (82). Thus, other known mechanisms of action which are independent of histone exposure, including decreases in ICAM-1 expression and suppression of membrane permeability, may also contribute to salutary benefits of suramin we observed.

In summary, we demonstrate a new and previously unreported mechanism of action for suramin. Suramin blocks cytotoxic effects of histones and prevents histone-induced vasodilatory dysfunction, endothelial cell activation, thrombin generation, lung injury, and mortality in mice. Our results provide a mechanistic basis and rationale for clinical trials of suramin as a repurposed treatment that can be rapidly deployed to prevent endothelial injury and excessive blood clotting in conditions associated with high circulating histone levels such as trauma and sepsis.

Supplementary Material

Refer to Web version on PubMed Central for supplementary material.

Acknowledgments

We thank Dr. Roxana Del Rio Guerra and the University of Vermont Larner College of Medicine Flow Cytometry and Cell Sorting Facility for extensive support on all flow cytometry experiments as well for instrumentation.

Financial Support

Research reported in this publication was supported by the Totman Medical Research Trust (to M.T.N.), the European Union Horizon 2020 Research and Innovation Programme (Grant Agreement 666881, SVDs@target, to M.T.N.), as well as grants from the National Institute of Neurological Disorders and Stroke (NINDS) and National Institute of Aging (NIA) (R01-NS-110656 to M.T.N.), the National Institute of General Medical Sciences (NIGMS) (P20-GM-135007 to M.T.N and R35-GM-144099-01 to K.F.), and the National Heart, Lung, and Blood Institute (NHLBI) (R01-HL-146914 to S.S., R01-HL-157407 to S.S., R01-HL-142081 to M.E.P, R01-HL-133920 to M.E.P., R35-HL-140027 to M.T.N., and 1OT2HL156812 to K.F.); the Department of Defense/ The Henry M. Jackson Foundation for the Advancement of Military Medicine (HU001-18-2-0016 to K.F.); the Office of the Director, National Institutes of Health (S10-OD-026843 to J.E.B.); the National Institute of Allergy and Infectious Diseases (R03-AI153902 to J.E.B); and the American Chemical Society (ACS-PRF-58219-DNI to J.L. and Y.T). Imaging work was performed at the Microscopy Imaging Center at the University of Vermont (RRID# SCR_018821). The views and conclusions contained in this document are those of the authors and should not be interpreted as representing the official policies, either expressed or implied, of the NIH.

References

1. Gu SX, Tyagi T, Jain K, Gu VW, Lee SH, Hwa JM, Kwan JM, Krause DS, Lee AI, Halene S, Martin KA, Chun HJ, and Hwa J. 2021. Thrombocytopathy and endotheliopathy: crucial contributors to COVID-19 thromboinflammation. Nat. Rev. Cardiol 18: 194–209. [PubMed: 33214651]
2. Barrett TJ, Cornwell M, Myndzar K, Rolling CC, Xia Y, Drenkova K, Biebuyck A, Fields AT, Tawil M, Luttrell-Williams E, Yuriditsky E, Smith G, Cotzia P, Neal MD, Kornblith LZ, Pittaluga S, Rapkiewicz AV, Burgess HM, Mohr I, Stapleford KA, Voora D, Ruggles K, Hochman J, and Berger JS. Platelets amplify endotheliopathy in COVID-19. Sci. Adv 7: eabh2434.
3. Xu J, Zhang X, Pelayo R, Monestier M, Ammollo CT, Semeraro F, Taylor FB, Esmon NL, Lupu F, and Esmon CT. 2009. Extracellular histones are major mediators of death in sepsis. Nat. Med 15: 1318–1321. [PubMed: 19855397]
4. Schumski A, Ortega-Gómez A, Wichapong K, Winter C, Lemnitzer P, Viola JR, Pinilla-Vera M, Folco E, Solis-Mezarino V, Völker-Albert M, Maas SL, Pan C, Perez Olivares L, Winter J, Hackeng T, Karlsson MCI, Zeller T, Imhof A, Baron RM, Nicolaes GAF, Libby P, Maegdefessel L, Kamp F, Benoit M, Döring Y, and Soehnlein O. 2021. Endotoxinemia Accelerates Atherosclerosis Through Electrostatic Charge–Mediated Monocyte Adhesion. Circulation 143: 254–266. [PubMed: 33167684]
5. Wu D, Ingram A, Lahti JH, Mazza B, Grenet J, Kapoor A, Liu L, Kidd VJ, and Tang D. 2002. Apoptotic release of histones from nucleosomes. J. Biol. Chem 277: 12001–12008.
6. Allam R, Scherbaum CR, Darisipudi MN, Mulay SR, Hägele H, Lichtnekert J, Hagemann JH, Rupanagudi KV, Ryu M, Schwarzenberger C, Hohenstein B, Hugo C, Uhl B, Reichel CA, Krombach F, Monestier M, Liapis H, Moreth K, Schaefer L, and Anders H-J. 2012. Histones from dying renal cells aggravate kidney injury via TLR2 and TLR4. J. Am. Soc. Nephrol. JASN 23: 1375–1388. [PubMed: 22677551]
7. Wickman GR, Julian L, Mardilovich K, Schumacher S, Munro J, Rath N, Zander SA, Mleczak A, Sumpton D, Morrice N, Bienvenut WV, and Olson MF. 2013. Blebs produced by actin-myosin contraction during apoptosis release damage-associated molecular pattern proteins before secondary necrosis occurs. Cell Death Differ. 20: 1293–1305. [PubMed: 23787996]
8. Tsourouktsoglou T-D, Warnatsch A, Ioannou M, Hoving D, Wang Q, and Papayannopoulos V. 2020. Histones, DNA, and Citrullination Promote Neutrophil Extracellular Trap Inflammation by Regulating the Localization and Activation of TLR4. Cell Rep. 31: 107602.

9. Zuo Y, Yalavarthi S, Navaz SA, Hoy CK, Harbaugh A, Gockman K, Zuo M, Madison JA, Shi H, Kanthi Y, and Knight JS. 2021. Autoantibodies stabilize neutrophil extracellular traps in COVID-19. JCI Insight 6: 150111.
10. Knight JS, Luo W, O'Dell AA, Yalavarthi S, Zhao W, Subramanian V, Guo C, Grenn RC, Thompson PR, Eitzman DT, and Kaplan MJ. 2014. Peptidylarginine deiminase inhibition reduces vascular damage and modulates innate immune responses in murine models of atherosclerosis. Circ. Res 114: 947–956. [PubMed: 24425713]
11. Silvestre-Roig C, Braster Q, Wichapong K, Lee EY, Teulon JM, Berrebeh N, Winter J, Adrover JM, Santos GS, Froese A, Lemnitzer P, Ortega-Gómez A, Chevre R, Marschner J, Schumski A, Winter C, Perez-Olivares L, Pan C, Paulin N, Schoufour T, Hartwig H, González-Ramos S, Kamp F, Megens RTA, Mowen KA, Gunzer M, Maegdefessel L, Hackeng T, Lutgens E, Daemen M, von Blume J, Anders H-J, Nikolaev VO, Pellequer J-L, Weber C, Hidalgo A, Nicolaes GAF, Wong GCL, and Soehnlein O. 2019. Externalized histone H4 orchestrates chronic inflammation by inducing lytic cell death. Nature 569: 236–240. [PubMed: 31043745]
12. Savchenko AS, Borissoff JI, Martinod K, De Meyer SF, Gallant M, Erpenbeck L, Brill A, Wang Y, and Wagner DD. 2014. VWF-mediated leukocyte recruitment with chromatin decondensation by PAD4 increases myocardial ischemia/reperfusion injury in mice. Blood 123: 141–148. [PubMed: 24200682]
13. Brill A, Fuchs TA, Savchenko AS, Thomas GM, Martinod K, De Meyer SF, Bhandari AA, and Wagner DD. 2012. Neutrophil extracellular traps promote deep vein thrombosis in mice. J. Thromb. Haemost. JTH 10: 136–144. [PubMed: 22044575]
14. Savchenko AS, Martinod K, Seidman MA, Wong SL, Borissoff JI, Piazza G, Libby P, Goldhaber SZ, Mitchell RN, and Wagner DD. 2014. Neutrophil extracellular traps form predominantly during the organizing stage of human venous thromboembolism development. J. Thromb. Haemost. JTH 12: 860–870. [PubMed: 24674135]
15. Marsman G, Zeerleder S, and Luken BM. 2016. Extracellular histones, cell-free DNA, or nucleosomes: differences in immunostimulation. Cell Death Dis. 7: e2518.
16. Silk E, Zhao H, Weng H, and Ma D. 2017. The role of extracellular histone in organ injury. Cell Death Dis. 8: e2812.
17. Nakazawa D, Kumar SV, Marschner J, Desai J, Holderied A, Rath L, Kraft F, Lei Y, Fukasawa Y, Moeckel GW, Angelotti ML, Liapis H, and Anders H-J. 2017. Histones and Neutrophil Extracellular Traps Enhance Tubular Necrosis and Remote Organ Injury in Ischemic AKI. J. Am. Soc. Nephrol. JASN 28: 1753–1768. [PubMed: 28073931]
18. Shaw RJ, Abrams ST, Austin J, Taylor JM, Lane S, Dutt T, Downey C, Du M, Turtle L, Baillie JK, Openshaw PJM, Wang G, Semple MG, and Toh C-H. 2021. Circulating histones play a central role in COVID-19-associated coagulopathy and mortality. Haematologica 106: 2493–2498. [PubMed: 33832219]
19. Abrams ST, Zhang N, Manson J, Liu T, Dart C, Baluwa F, Wang SS, Brohi K, Kipar A, Yu W, Wang G, and Toh C-H. 2013. Circulating Histones Are Mediators of Trauma-associated Lung Injury. Am. J. Respir. Crit. Care Med. 187: 160–169. [PubMed: 23220920]
20. Collier DM, Villalba N, Sackheim A, Bonev AD, Miller ZD, Moore JS, Shui B, Lee JC, Lee FK, Reining S, Kotlikoff MI, Nelson MT, and Freeman K. 2019. Extracellular histones induce calcium signals in the endothelium of resistance-sized mesenteric arteries and cause loss of endothelium-dependent dilation. Am. J. Physiol. Heart Circ. Physiol 316: H1309–H1322. [PubMed: 30848676]
21. Yeung KW, Lau PM, Tsang HL, Ho HP, Kwan YW, and Kong SK. 2019. Extracellular Histones Induced Eryptotic Death in Human Erythrocytes. Cell. Physiol. Biochem. Int. J. Exp. Cell. Physiol. Biochem. Pharmacol 53: 229–241.
22. Connor H O' Meara, Coupland LA, Kordbacheh F, Quah BJC, Chang C-W, Simon Davis DA, Bezos A, Browne AM, Freeman C, Hammill DJ, Chopra P, Pipa G, Madge PD, Gallant E, Segovis C, Dulhunty AF, Arnolda LF, Mitchell I, Khachigian LM, Stephens RW, von Itzstein M, and Parish CR. 2020. Neutralizing the pathological effects of extracellular histones with small polyanions. Nat. Commun 11: 6408. [PubMed: 33328478]
23. Villalba N, Baby S, Cha BJ, and Yuan SY. 2020. Site-specific opening of the blood-brain barrier by extracellular histones. J. Neuroinflammation 17: 281. [PubMed: 32962721]

24. Allam R, Darisipudi MN, Tschopp J, and Anders H-J. 2013. Histones trigger sterile inflammation by activating the NLRP3 inflammasome. Eur. J. Immunol 43: 3336–3342. [PubMed: 23964013]
25. Semeraro F, Ammollo CT, Morrissey JH, Dale GL, Friese P, Esmon NL, and Esmon CT. 2011. Extracellular histones promote thrombin generation through platelet-dependent mechanisms: involvement of platelet TLR2 and TLR4. Blood 118: 1952–1961. [PubMed: 21673343]
26. Shi C-X, Wang Y, Chen Q, Jiao F-Z, Pei M-H, and Gong Z-J. 2020. Extracellular Histone H3 Induces Pyroptosis During Sepsis and May Act Through NOD2 and VSIG4/NLRP3 Pathways. Front. Cell. Infect. Microbiol 10: 196. [PubMed: 32432055]
27. Yang X, Li L, Liu J, Lv B, and Chen F. 2016. Extracellular histones induce tissue factor expression in vascular endothelial cells via TLR and activation of NF-κB and AP-1. Thromb. Res 137: 211–218. [PubMed: 26476743]
28. Meegan JE, Yang X, Beard RS, Jannaway M, Chatterjee V, Taylor-Clark TE, and Yuan SY. 2018. Citrullinated Histone 3 Causes Endothelial Barrier Dysfunction. Biochem. Biophys. Res. Commun 503: 1498–1502. [PubMed: 30029877]
29. Pereira LF, Marco FM, Boimorto R, Caturla A, Bustos A, De la Concha EG, and Subiza JL. 1994. Histones interact with anionic phospholipids with high avidity; its relevance for the binding of histone-antihistone immune complexes. Clin. Exp. Immunol 97: 175–180. [PubMed: 8050163]
30. Sakharov DV, Jie AF, Bekkers ME, Emeis JJ, and Rijken DC. 2001. Polylysine as a vehicle for extracellular matrix-targeted local drug delivery, providing high accumulation and long-term retention within the vascular wall. Arterioscler. Thromb. Vasc. Biol 21: 943–948. [PubMed: 11397701]
31. Vulliamy P, Gillespie S, Armstrong PC, Allan HE, Warner TD, and Brohi K. 2019. Histone H4 induces platelet ballooning and microparticle release during trauma hemorrhage. Proc. Natl. Acad. Sci. U. S. A 116: 17444–17449.
32. Henriksen HH, McGarrity S, SigurÐardóttir RS, Nemkov T, D'Alessandro A, Palsson BO, Stensballe J, Wade CE, Rolfsson Ó, and Johansson PI. 2020. Metabolic Systems Analysis of Shock-Induced Endotheliopathy (SHINE) in Trauma: A New Research Paradigm. Ann. Surg 272: 1140–1148. [PubMed: 31274658]
33. Johansson PI, Henriksen HH, Stensballe J, Gybel-Brask M, Cardenas JC, Baer LA, Cotton BA, Holcomb JB, Wade CE, and Ostrowski SR. 2017. Traumatic Endotheliopathy: A Prospective Observational Study of 424 Severely Injured Patients. Ann. Surg 265: 597–603. [PubMed: 27144442]
34. Johansson PI, Windeløv NA, Rasmussen LS, Sørensen AM, and Ostrowski SR. 2013. Blood levels of histone-complexed DNA fragments are associated with coagulopathy, inflammation and endothelial damage early after trauma. J. Emerg. Trauma Shock 6: 171–175. [PubMed: 23960372]
35. Kutcher ME, Xu J, Vilardi RF, Ho C, Esmon CT, and Cohen MJ. 2012. Extracellular histone release in response to traumatic injury: implications for a compensatory role of activated Protein C. J. Trauma Acute Care Surg. 73.
36. Naumann DN, Hazeldine J, Davies DJ, Bishop J, Midwinter MJ, Belli A, Harrison P, and Lord JM. 2018. Endotheliopathy of Trauma is an on-Scene Phenomenon, and is Associated with Multiple Organ Dysfunction Syndrome: A Prospective Observational Study. Shock 49: 420–428. [PubMed: 28945676]
37. Naumann DN, Hazeldine J, Dinsdale RJ, Bishop JR, Midwinter MJ, Harrison P, Hutchings SD, and Lord JM. 2017. Endotheliopathy is associated with higher levels of cell-free DNA following major trauma: A prospective observational study. PloS One 12: e0189870.
38. Russell RT, Christiaans SC, Nice TR, Banks M, Mortellaro VE, Morgan C, Duhachek-Stapelman A, Lisco SJ, Kerby JD, Wagener BM, Chen MK, and Pittet J-F. 2018. Histone-Complexed DNA Fragments Levels are Associated with Coagulopathy, Endothelial Cell Damage, and Increased Mortality after Severe Pediatric Trauma. Shock Augusta Ga 49: 44–52. [PubMed: 28509684]
39. McCullough LD, Roy-O'Reilly M, Lai Y-J, Patrizz A, Xu Y, Lee J, Holmes A, Kraushaar DC, Chauhan A, Sansing LH, Stonestreet BS, Zhu L, Kofler J, Lim Y-P, and Venna VR. 2021. Exogenous inter-α inhibitor proteins prevent cell death and improve ischemic stroke outcomes in mice. J. Clin. Invest 131.

40. Yang R, Tenhunen J, and Tonnessen TI. 2017. HMGB1 and Histones Play a Significant Role in Inducing Systemic Inflammation and Multiple Organ Dysfunctions in Severe Acute Pancreatitis. Int. J. Inflamm 2017: 1817564.
41. Lv X, Wen T, Song J, Xie D, Wu L, Jiang X, Jiang P, and Wen Z. 2017. Extracellular histones are clinically relevant mediators in the pathogenesis of acute respiratory distress syndrome. Respir. Res 18: 165. [PubMed: 28865478]
42. Zhang Y, Wen Z, Guan L, Jiang P, Gu T, Zhao J, Lv X, and Wen T. 2015. Extracellular Histones Play an Inflammatory Role in Acid Aspiration-induced Acute Respiratory Distress Syndrome. Anesthesiology 122: 127–139. [PubMed: 25188000]
43. Pati S, Fennern E, Holcomb JB, Barry M, Trivedi A, Cap AP, Martin MJ, Wade C, Kozar R, Cardenas JC, Rappold JF, Spiegel R, and Schreiber MA. 2021. Treating the endotheliopathy of SARS-CoV-2 infection with plasma: Lessons learned from optimized trauma resuscitation with blood products. Transfusion (Paris) 61 Suppl 1: S336–S347.
44. Shi H, Gandhi AA, Smith SA, Wang Q, Chiang D, Yalavarthi S, Ali RA, Liu C, Sule G, Tsou P-S, Zuo Y, Kanthi Y, Farkash EA, Lin JD, Morrissey JH, and Knight JS. 2021. Endothelium-protective, histone-neutralizing properties of the polyanionic agent defibrotide. JCI Insight 6.
45. Pope WJ 1924. SYNTHETIC THERAPEUTIC AGENTS. Br. Med. J 1: 413–414. [PubMed: 20771495]
46. Daneva Z, Ottolini M, Chen YL, Klimentova E, Kuppusamy M, Shah SA, Minshall RD, Seye CI, Laubach VE, Isakson BE, and Sonkusare SK. 2021. Endothelial pannexin 1-TRPV4 channel signaling lowers pulmonary arterial pressure in mice. eLife 10: e67777.
47. Sonkusare SK, Bonev AD, Ledoux J, Liedtke W, Kotlikoff MI, Heppner TJ, Hill-Eubanks DC, and Nelson MT. 2012. Elementary Ca2+ signals through endothelial TRPV4 channels regulate vascular function. Science 336: 597–601. [PubMed: 22556255]
48. Liao C, Esai Selvan M, Zhao J, Slimovitch JL, Schneebeli ST, Shelley M, Shelley JC, and Li J. 2015. Melittin Aggregation in Aqueous Solutions: Insight from Molecular Dynamics Simulations. J. Phys. Chem. B 119: 10390–10398.
49. Li J, McKay KT, Remington JM, and Schneebeli ST. 2021. A computational study of cooperative binding to multiple SARS-CoV-2 proteins. Sci. Rep 11: 16307.
50. Bouchard BA, and Freeman K. 2021. Thrombin Formation. In Trauma Induced Coagulopathy Moore HB, Neal MD, and Moore EE, eds. Springer International Publishing, Cham. 77–84.
51. Malkin EZ, and Bratman SV. 2020. Bioactive DNA from extracellular vesicles and particles. Cell Death Dis. 11: 584. [PubMed: 32719324]
52. Kleine TJ, Gladfelter A, Lewis PN, and Lewis SA. 1995. Histone-induced damage of a mammalian epithelium: the conductive effect. Am. J. Physiol 268: C1114–1125.
53. Gamberucci A, Fulceri R, Marcolongo P, Pralong WF, and Benedetti A. 1998. Histones and basic polypeptides activate Ca2+/cation influx in various cell types. Biochem. J 331 (Pt 2): 623–630. [PubMed: 9531506]
54. Lam FW, Cruz MA, Parikh K, and Rumbaut RE. 2016. Histones stimulate von Willebrand factor release in vitro and in vivo. Haematologica 101: e277–e279. [PubMed: 27013650]
55. Kim JE, Yoo HJ, Gu JY, and Kim HK. 2016. Histones Induce the Procoagulant Phenotype of Endothelial Cells through Tissue Factor Up-Regulation and Thrombomodulin Down-Regulation. PloS One 11: e0156763.
56. Ammollo CT, Semeraro F, Xu J, Esmon NL, and Esmon CT. 2011. Extracellular histones increase plasma thrombin generation by impairing thrombomodulin-dependent protein C activation. J. Thromb. Haemost. JTH 9: 1795–1803. [PubMed: 21711444]
57. Yang H, Kim A, David T, Palmer D, Jin T, Tien J, Huang F, Cheng T, Coughlin SR, Jan YN, and Jan LY. 2012. TMEM16F forms a Ca2+-activated cation channel required for lipid scrambling in platelets during blood coagulation. Cell 151: 111–122. [PubMed: 23021219]
58. Gao C, Xie R, Yu C, Ma R, Dong W, Meng H, Zhang Y, Si Y, Zhang Z, Novakovic V, Zhang Y, Kou J, Bi Y, Li B, Xie R, Gilbert GE, Zhou J, and Shi J. 2015. Thrombotic Role of Blood and Endothelial Cells in Uremia through Phosphatidylserine Exposure and Microparticle Release. PloS One 10: e0142835.

59. Wildhagen KCAA, García de Frutos P, Reutelingsperger CP, Schrijver R, Aresté C, Ortega-Gómez A, Deckers NM, Hemker HC, Soehnlein O, and Nicolaes GAF. 2014. Nonanticoagulant heparin prevents histone-mediated cytotoxicity in vitro and improves survival in sepsis. Blood 123: 1098–1101. [PubMed: 24264231]

60. Iba T, Hashiguchi N, Nagaoka I, Tabe Y, Kadota K, and Sato K. 2015. Heparins attenuated histone-mediated cytotoxicity in vitro and improved the survival in a rat model of histone-induced organ dysfunction. Intensive Care Med. Exp 3: 36.

61. Pal PK, Starr T, and Gertler MM. 1983. Neutralization of heparin by histone and its subfractions. Thromb. Res 31: 69–79. [PubMed: 6612698]

62. REMAP-CAP Investigators, ACTIV-4a Investigators, ATTACC Investigators, Goligher EC, Bradbury CA, McVerry BJ, Lawler PR, Berger JS, Gong MN, Carrier M, Reynolds HR, Kumar A, Turgeon AF, Kornblith LZ, Kahn SR, Marshall JC, Kim KS, Houston BL, Derde LPG, Cushman M, Tritschler T, Angus DC, Godoy LC, McQuilten Z, Kirwan B-A, Farkouh ME, Brooks MM, Lewis RJ, Berry LR, Lorenzi E, Gordon AC, Ahuja T, Al-Beidh F, Annane D, Arabi YM, Aryal D, Baumann Kreuziger L, Beane A, Bhimani Z, Bihari S, Billett HH, Bond L, Bonten M, Brunkhorst F, Buxton M, Buzgau A, Castellucci LA, Chekuri S, Chen J-T, Cheng AC, Chkhikvadze T, Coiffard B, Contreras A, Costantini TW, de Brouwer S, Detry MA, Duggal A, Džavík V, Effron MB, Eng HF, Escobedo J, Estcourt LJ, Everett BM, Fergusson DA, Fitzgerald M, Fowler RA, Froess JD, Fu Z, Galanaud JP, Galen BT, Gandotra S, Girard TD, Goodman AL, Goossens H, Green C, Greenstein YY, Gross PL, Haniffa R, Hegde SM, Hendrickson CM, Higgins AM, Hindenburg AA, Hope AA, Horowitz JM, Horvat CM, Huang DT, Hudock K, Hunt BJ, Husain M, Hyzy RC, Jacobson JR, Jayakumar D, Keller NM, Khan A, Kim Y, Kindzelski A, King AJ, Knudson MM, Kornblith AE, Kutcher ME, Laffan MA, Lamontagne F, Le Gal G, Leeper CM, Leifer ES, Lim G, Gallego Lima F, Linstrum K, Litton E, Lopez-Sendon J, Lother SA, Marten N, Saud Marinez A, Martinez M, Mateos Garcia E, Mavromichalis S, McAuley DF, McDonald EG, McGlothlin A, McGuinness SP, Middeldorp S, Montgomery SK, Mouncey PR, Murthy S, Nair GB, Nair R, Nichol AD, Nicolau JC, Nunez-Garcia B, Park JJ, Park PK, Parke RL, Parker JC, Parnia S, Paul JD, Pompilio M, Quigley JG, Rosenson RS, Rost NS, Rowan K, Santos FO, Santos M, Santos MO, Satterwhite L, Saunders CT, Schreiber J, Schutgens REG, Seymour CW, Siegal DM, Silva DG, Singhal AB, Slutsky AS, Solvason D, Stanworth SJ, Turner AM, van Bentum-Puijk W, van de Veerdonk FL, van Diepen S, Vazquez-Grande G, Wahid L, Wareham V, Widmer RJ, Wilson JG, Yuriditsky E, Zhong Y, Berry SM, McArthur CJ, Neal MD, Hochman JS, Webb SA, and Zarychanski R. 2021. Therapeutic Anticoagulation with Heparin in Critically Ill Patients with Covid-19. N. Engl. J. Med 385: 777–789. [PubMed: 34351722]

63. ATTACC Investigators, ACTIV-4a Investigators, REMAP-CAP Investigators, Lawler PR, Goligher EC, Berger JS, Neal MD, McVerry BJ, Nicolau JC, Gong MN, Carrier M, Rosenson RS, Reynolds HR, Turgeon AF, Escobedo J, Huang DT, Bradbury CA, Houston BL, Kornblith LZ, Kumar A, Kahn SR, Cushman M, McQuilten Z, Slutsky AS, Kim KS, Gordon AC, Kirwan B-A, Brooks MM, Higgins AM, Lewis RJ, Lorenzi E, Berry SM, Berry LR, Aday AW, Al-Beidh F, Annane D, Arabi YM, Aryal D, Baumann Kreuziger L, Beane A, Bhimani Z, Bihari S, Billett HH, Bond L, Bonten M, Brunkhorst F, Buxton M, Buzgau A, Castellucci LA, Chekuri S, Chen J-T, Cheng AC, Chkhikvadze T, Coiffard B, Costantini TW, de Brouwer S, Derde LPG, Detry MA, Duggal A, Džavík V, Effron MB, Estcourt LJ, Everett BM, Fergusson DA, Fitzgerald M, Fowler RA, Galanaud JP, Galen BT, Gandotra S, García-Madrona S, Girard TD, Godoy LC, Goodman AL, Goossens H, Green C, Greenstein YY, Gross PL, Hamburg NM, Haniffa R, Hanna G, Hanna N, Hegde SM, Hendrickson CM, Hite RD, Hindenburg AA, Hope AA, Horowitz JM, Horvat CM, Hudock K, Hunt BJ, Husain M, Hyzy RC, Iyer VN, Jacobson JR, Jayakumar D, Keller NM, Khan A, Kim Y, Kindzelski AL, King AJ, Knudson MM, Kornblith AE, Krishnan V, Kutcher ME, Laffan MA, Lamontagne F, Le Gal G, Leeper CM, Leifer ES, Lim G, Lima FG, Linstrum K, Litton E, Lopez-Sendon J, Lopez-Sendon Moreno JL, Lother SA, Malhotra S, Marcos M, Saud Marinez A, Marshall JC, Marten N, Matthay MA, McAuley DF, McDonald EG, McGlothlin A, McGuinness SP, Middeldorp S, Montgomery SK, Moore SC, Morillo Guerrero R, Mouncey PR, Murthy S, Nair GB, Nair R, Nichol AD, Nunez-Garcia B, Pandey A, Park PK, Parke RL, Parker JC, Parnia S, Paul JD, Pérez González YS, Pompilio M, Prekker ME, Quigley JG, Rost NS, Rowan K, Santos FO, Santos M, Olombrada Santos M, Satterwhite L, Saunders CT, Schutgens REG, Seymour CW, Siegal DM, Silva DG, Shankar-Hari M, Sheehan JP, Singhal AB, Solvason D, Stanworth SJ, Tritschler T, Turner AM, van Bentum-Puijk W, van de Veerdonk FL, van Diepen

S, Vazquez-Grande G, Wahid L, Wareham V, Wells BJ, Widmer RJ, Wilson JG, Yuriditsky E, Zampieri FG, Angus DC, McArthur CJ, Webb SA, Farkouh ME, Hochman JS, and Zarychanski R. 2021. Therapeutic Anticoagulation with Heparin in Noncritically Ill Patients with Covid-19. N. Engl. J. Med 385: 790–802. [PubMed: 34351721]

64. Horne MK, Wilson OJ, Cooper M, Gralnick HR, and Myers CE. 1992. The effect of suramin on laboratory tests of coagulation. Thromb. Haemost 67: 434–439. [PubMed: 1631791]
65. Daigo K, Nakakido M, Ohashi R, Fukuda R, Matsubara K, Minami T, Yamaguchi N, Inoue K, Jiang S, Naito M, Tsumoto K, and Hamakubo T. 2014. Protective effect of the long pentraxin PTX3 against histone-mediated endothelial cell cytotoxicity in sepsis. Sci. Signal 7: ra88.
66. Wygrecka M, Kosanovic D, Wujak L, Reppe K, Henneke I, Frey H, Didiasova M, Kwapiszewska G, Marsh LM, Baal N, Hackstein H, Zakrzewicz D, Müller-Redetzky HC, de Maat S, Maas C, Nolte MW, Panousis C, Schermuly RT, Seeger W, Witzenrath M, Schaefer L, and Markart P. 2017. Antihistone Properties of C1 Esterase Inhibitor Protect against Lung Injury. Am. J. Respir. Crit. Care Med. 196: 186–199. [PubMed: 28005404]
67. Lam FW, Cruz MA, Leung H-CE, Parikh KS, Smith CW, and Rumbaut RE. 2013. Histone induced platelet aggregation is inhibited by normal albumin. Thromb. Res 132: 69–76. [PubMed: 23673386]
68. Bouchard BA, Colovos C, Lawson M, Osborn Z, Sackheim A, Mould KJ, Janssen WJ, Cohen MJ, Majumdar D, and Freeman K. 2021. Increased Histone-DNA Complexes and Endothelial-Dependent Thrombin Generation in Severe COVID-19,. ; :2021.07.03.450992.
69. Fatmi S, Taouzinet L, Skiba M, and Iguer-Ouada M. 2021. The Use of Cyclodextrin or its Complexes as a Potential Treatment Against the 2019 Novel Coronavirus: A Mini-Review. Curr. Drug Deliv. 18: 382–386. [PubMed: 32940180]
70. Jaimes F, De La Rosa G, Morales C, Fortich F, Arango C, Aguirre D, and Muñoz A. 2009. Unfractioned heparin for treatment of sepsis: A randomized clinical trial (The HETRASE Study). Crit. Care Med. 37: 1185–1196. [PubMed: 19242322]
71. Sayburn A 2020. Covid-19: trials of four potential treatments to generate “robust data” of what works. BMJ 368: m1206.
72. Zhu W, Xu M, Chen CZ, Guo H, Shen M, Hu X, Shinn P, Klumpp-Thomas C, Michael SG, and Zheng W. 2020. Identification of SARS-CoV-2 3CL Protease Inhibitors by a Quantitative High-Throughput Screening. ACS Pharmacol. Transl. Sci 3: 1008–1016. [PubMed: 33062953]
73. Waldhoer M, Bofill-Cardona E, Milligan G, Freissmuth M, and Nanoff C. 1998. Differential uncoupling of A1 adenosine and D2 dopamine receptors by suramin and didemethylated suramin (NF037). Mol. Pharmacol 53: 808–818. [PubMed: 9584206]
74. Lehmann N, Krishna Aradhyam G, and Fahmy K. 2002. Suramin affects coupling of rhodopsin to transducin. Biophys. J 82: 793–802. [PubMed: 11806921]
75. Hohenegger M, Matyash M, Poussu K, Herrmann-Frank A, Sarközi S, Lehmann-Horn F, and Freissmuth M. 1996. Activation of the skeletal muscle ryanodine receptor by suramin and suramin analogs. Mol. Pharmacol 50: 1443–1453. [PubMed: 8967964]
76. Leff P, Wood BE, and O’Connor SE. 1990. Suramin is a slowly-equilibrating but competitive antagonist at P2x-receptors in the rabbit isolated ear artery. Br. J. Pharmacol 101: 645–649. [PubMed: 2076483]
77. Manjula R, Anuja K, and Alcain FJ. 2020. SIRT1 and SIRT2 Activity Control in Neurodegenerative Diseases. Front. Pharmacol 11: 585821.
78. Lossos IS, Izbicki G, Or R, Goldstein RH, and Breuer R. 2000. The effect of suramin on bleomycin-induced lung injury. Life Sci. 67: 2873–2881. [PubMed: 11106002]
79. Rees S, Constantopoulos G, Barranger JA, and Brady RO. 1982. Organomegaly and histopathology in an animal model of mucopolysaccharidosis induced by suramin. Naunyn. Schmiedebergs Arch. Pharmacol 319: 262–270. [PubMed: 6810185]
80. Rees S, Constantopoulos G, and Brady RO. 1986. The suramin-treated rat as a model of mucopolysaccharidosis. Variation in the reversibility of biochemical and morphological changes among different organs. Virchows Arch. B Cell Pathol. Incl. Mol. Pathol 52: 259–272. [PubMed: 2879381]

81. Trieb K, Dorfinger K, Neuhold N, Selzer E, Wilfing A, Czernin S, Hermann M, Niederle B, Gessl A, and Vierhapper H. 1992. Suramin affects differentiated and undifferentiated human thyroid epithelial cells in vitro. J. Endocrinol 134: 505–511. [PubMed: 1357069]

82. Chi Y, Gao K, Zhang H, Takeda M, and Yao J. 2014. Suppression of cell membrane permeability by suramin: involvement of its inhibitory actions on connexin 43 hemichannels. Br. J. Pharmacol 171: 3448–3462. [PubMed: 24641330]

Key Points

- Histones produce acute thrombo-inflammatory responses of vascular endothelium
- Suramin protects small blood vessels from histone-induced damage

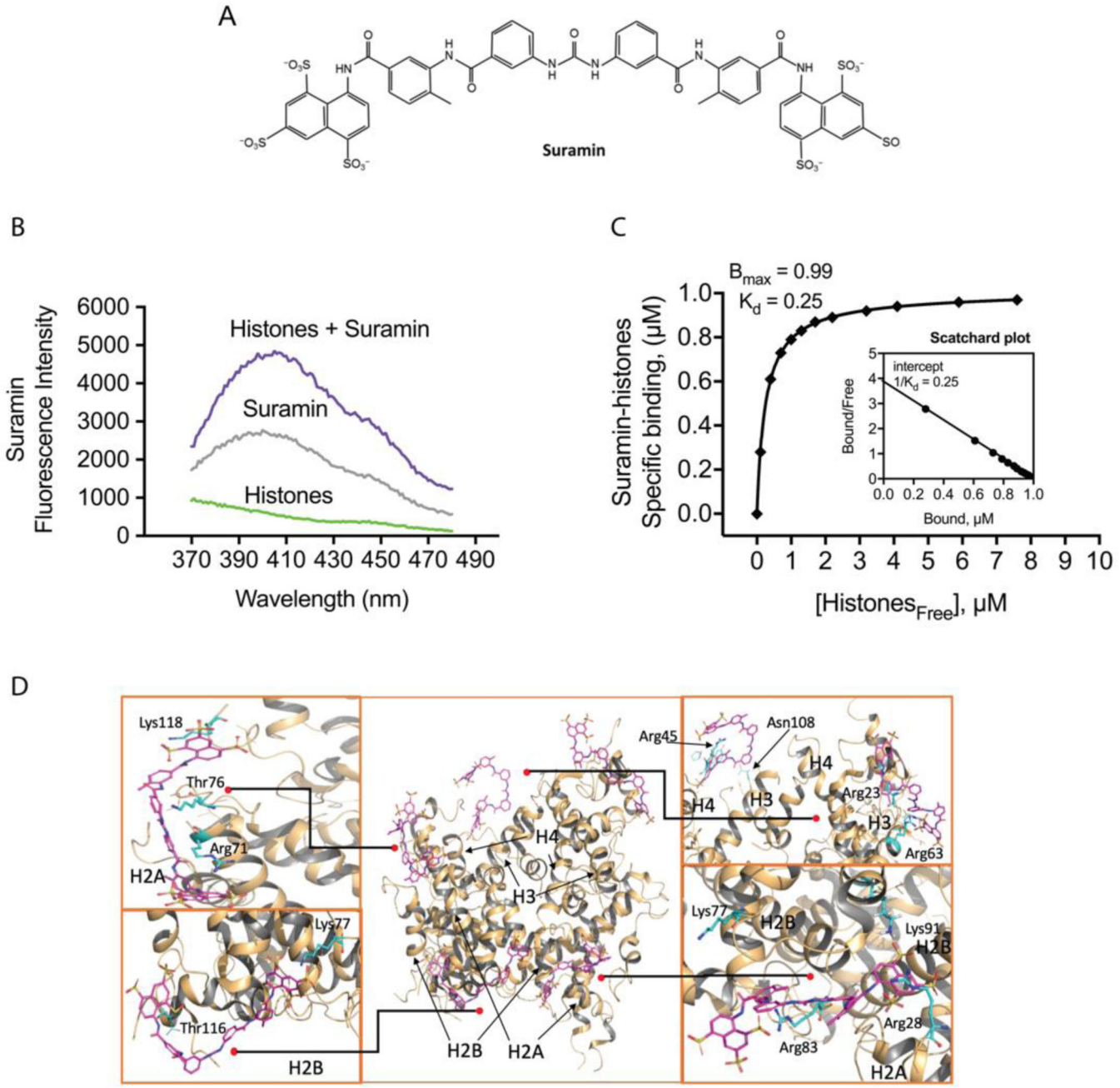

Figure 1.

Suramin binds histones in solution. (A) The chemical structure of suramin. (B) *In vitro* fluorescent spectroscopy studies were used to biochemically establish the interaction between suramin and histones. We established the absorbance and emission spectra for histones and suramin in solution (Supplemental Fig. 1 A), and then measured suramin sodium salt intrinsic fluorescence using increasing concentrations of suramin to determine the saturation range of the detector (Supplemental Fig. 1 B). (C) Scatchard plot analysis of the binding curve demonstrates a single high-affinity binding site with a dissociation constant (K_d) of 250 nM. (n=3 replicates for binding studies). (D) Molecular dynamics

simulations showing interactions between suramin molecules and the histone octamer in solution. Several exposed amino acid residues including arginine, asparagine, lysine, and threonine form hydrogen bonds with the sulfate groups on suramin (Lys118, Thr76, Arg71, Lys77, Thr116, Arg45, Asn108, Arg23, Arg63, Lys91, Arg83, Arg28). These include residues on H2A, H2B, H3, and H4, which are predicted to form stable electrostatic interactions with the sulfate groups on suramin.

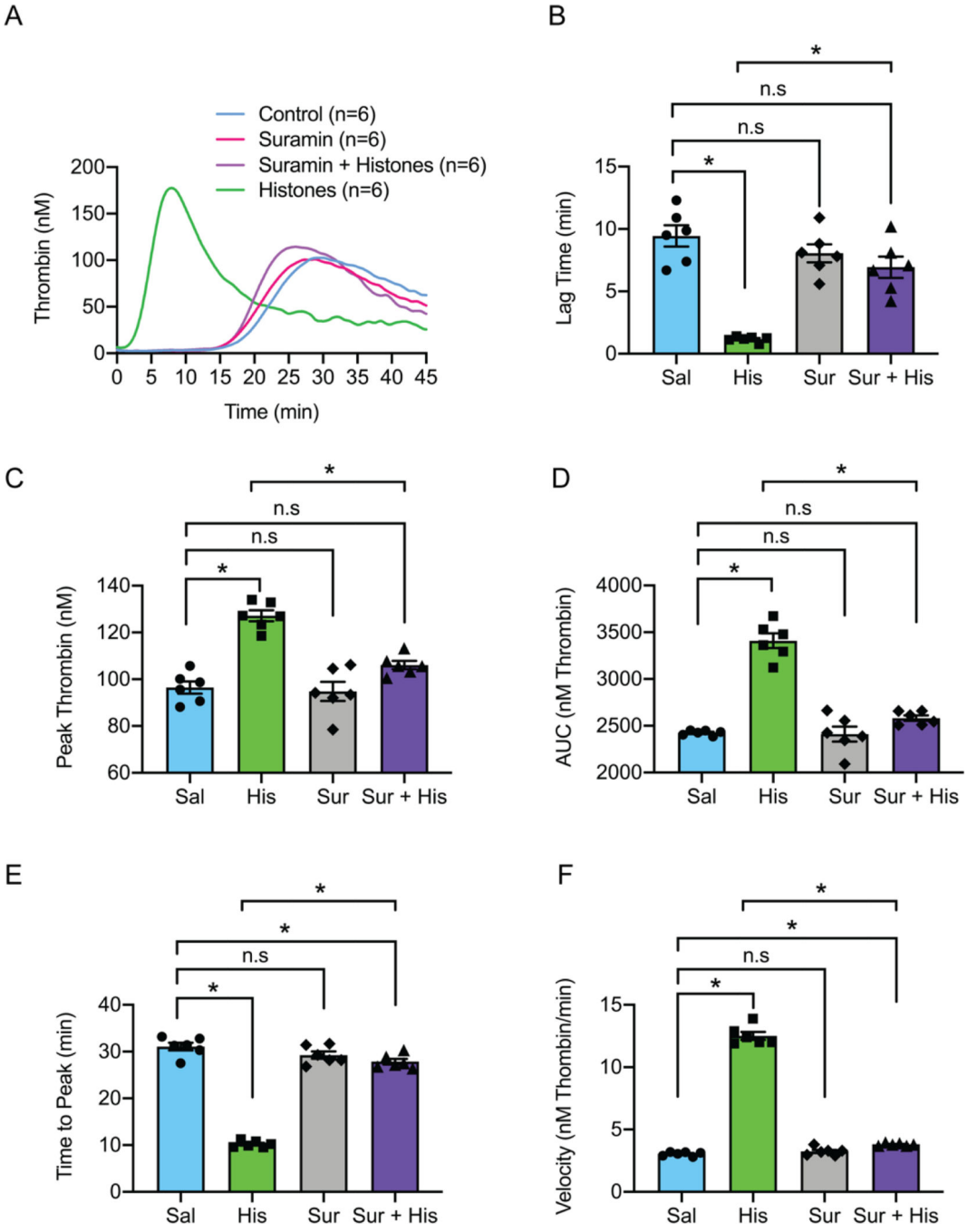

Figure 2.

Histones drive rapid thrombin generation on human endothelial cells which is blocked by suramin. (A) Calibrated automated thrombogram (CAT) tracings of thrombin generation (nM) vs time (min) by cultured human endothelial cells (Ea.hy926) in re-calcified, pooled, healthy human plasma. Histones (50 μg/mL), suramin (50 μM) or a combination of both were exogenously added to the cell culture and plasma samples as needed. (B) Summary data for lag time (min) in control (9 ± 0.8 min; n=6), suramin (8 ± 0.7 min; n=6), suramin and histones (67 ± 0.9 min; n=6) and histones (1 ± 0.1 min; n=6) samples. (C) Summary

data for peak thrombin (nM) in control (96 nM; n=6), suramin (94 ± 4 nM; n=6), suramin and histones (106 ± 2 nM; n=6) and histones (127 ± 2 nM; n=6) samples. (D) Summary data for area under the curve (AUC; nM thrombin) in control (143732 ± 2498 nM; n=6), suramin (139915 ± 2355 nM; n=6), suramin and histones (147896 ± 02968 nM; n=6) and histone (180248 ± 3977 nM; n=6) samples. (E) Summary data for time to peak (min) in control (31 ± 0.8 min; n=6), suramin (29 ± 0.8 min; n=6), suramin and histones (28 ± 0.6 min; n=6) and histone samples (10 ± 0.3 min; n=6). (F) Summary data for velocity (nM thrombin/min) in control (3.0 ± 0.1 nM thrombin/min; n=6), suramin (3.2 ± 0.1 nM thrombin/min; n=6), suramin and histones (3.8 ± 0.04 nM thrombin/min; n=6) and histone (13 ± 0.3 nM thrombin/min; n=6) samples. Data are expressed as mean ± SEM. Ordinary one-way ANOVA with Bonferroni's correction for multiple comparisons; $P<0.05$. A new biological replicate culture well was used for each group.

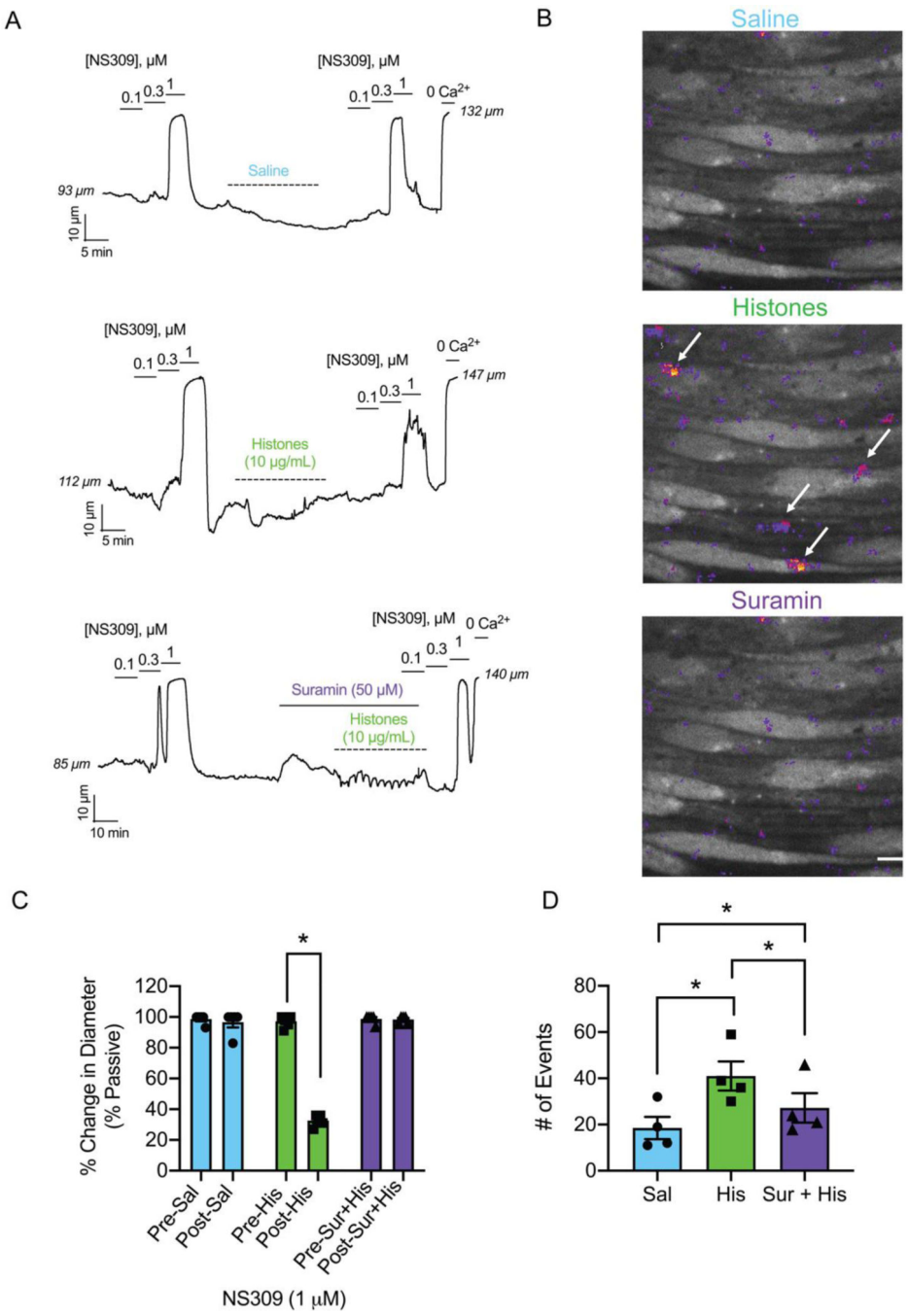

Figure 3.

Suramin prevents endothelial dysfunction and calcium overload caused by histones. (A) Representative tracings of pressurized (80 mm Hg), third-order, mouse mesenteric arteries. Histones (10 μg/mL) or saline (control) was flowed through the lumen at 2 μL/min (<5 dynes/cm^2) for 30 minutes. Dilations to the endothelial-dependent vasodilator NS309 (0.1; 0.3; 1 μM) pre-flow and post-flow were recorded. In one subset of experiments suramin (50 μM) was superfused abluminally for 10 minutes prior to and then continuously during histones flow. Maximal dilations were elicited at the end of the experiments using 0-Ca^{2+}

PSS. (B) Representative images from *en face* mouse pulmonary arteries loaded with Fluo-4 (10 μM) on a spinning disk confocal microscope. All images are from the same field of view recorded over 2 minutes. Arrows indicate large histone-induced calcium event F/F_0 ROIs. (C) Paired summary data of percent dilation to 1 μM NS309 pre-flow and post-flow of saline (pre-sal 99 ± 1 vs. post-sal 97 ± 3 %; n=5; n.s.), histones (10 μg/mL) (pre-his 97 ± 2 vs. post-his 33 ± 2 %; n=5; * $P<0.05$; Paired Student's T-test), and suramin (50 μM) with histones (pre-sur+his 99 ± 1 vs. post-sur-his 98 ± 1 %; n=5; n.s.). (D) Summary data of the paired total number of events per field after saline (control; 19 ± 5 events; n=4), histones (His; 10 μg/mL; 41 ± 6 events; n=4), and suramin (50 μM) and histones (Sur+His; 27 ± 6 events; n=4) application. Significant differences were determined using a repeated measures one-way ANOVA test with a Holm-Sidak correction for multiple comparisons for all three groups; $P<0.05$. Data are represented as mean ± SEM. Scale bar = 10 μm. A new biological replicate was used for each arteriography and calcium imaging experiment.

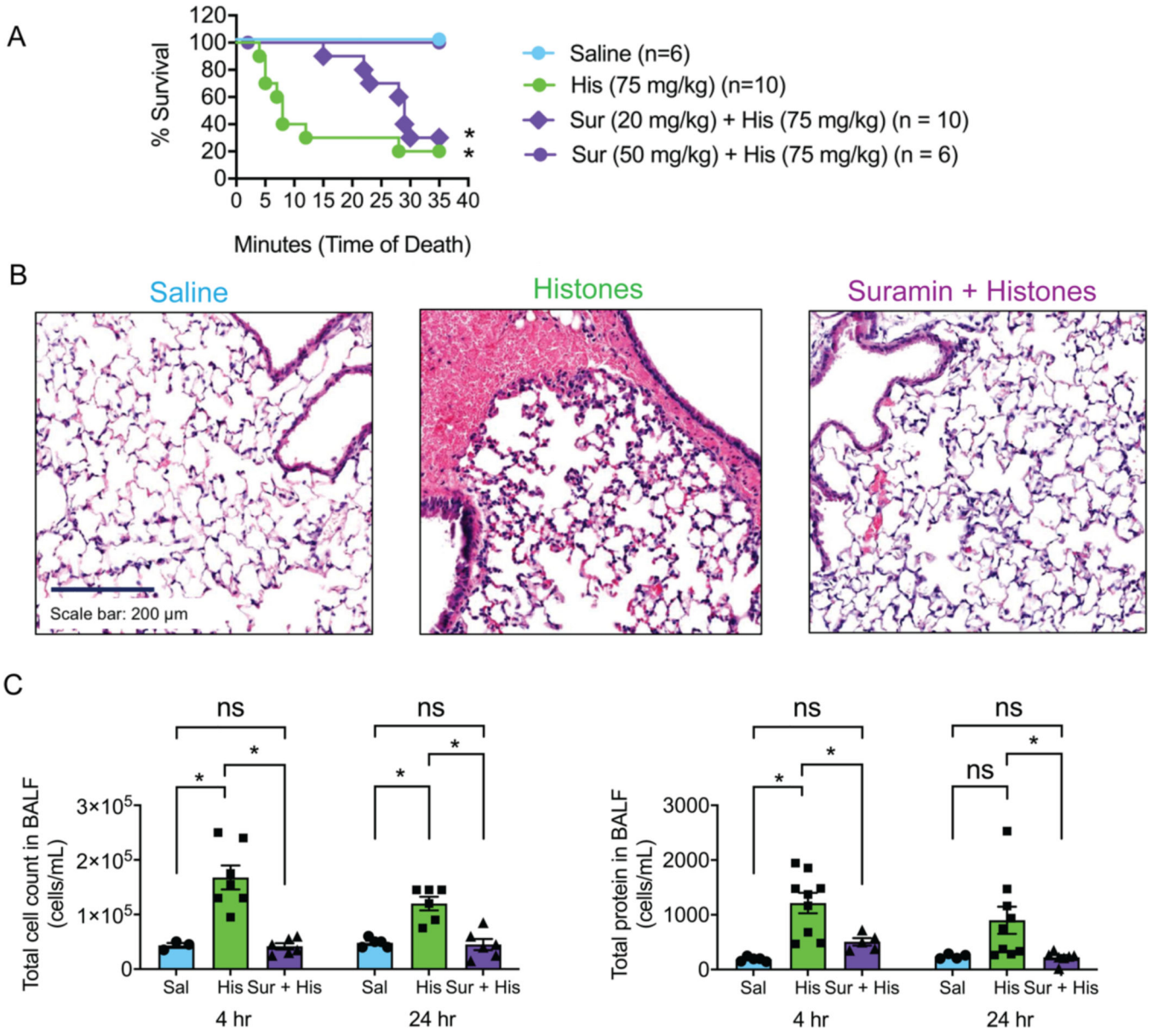

Figure 4.

Suramin improves survival and prevents lung injury and edema caused by histones. (A) Saline injected (control; n=6), a lethal dose of histones (His; 75 mg/Kg; n=10), and a lethal dose of histones with suramin (Sur+His; 20 mg/Kg n=11 or 50 mg/Kg n=6) was injected into mice and survival was recorded over the course of 35 minutes. Suramin was injected intraperitoneally. Mantel-Cox test; $P<0.05$; *, for each group compared to saline. (B) Representative images of hematoxylin and eosin stain (H&E) of a histological section of paraffin-embedded fixed lung tissue from a mouse from saline, histone, and suramin + histone treated groups (n=3). The dark blue color denotes cell nuclei, light pink extracellular matrix, and the red erythrocytes. Scale bar = 200 µm. (C) Summary data of the total, non-differentiated cell counts in the bronchial-alveolar lavage fluid (BALF) at 4 hours after saline (control; 43333 ± 4410 cells/mL; n=3), histones (His; 45 mg/Kg; 167847 ±

22008 cells/mL; n=7), or suramin (50 mg/Kg and histone injection (Sur+His; 41667 ± 5725 cells/mL; n=6) and 24 hours after saline (control; 48000 ± 3742 cells/mL; n=5), histones (His; 45 mg/Kg; 120000 ± 12649 cells/mL; n=6), or suramin (50 mg/Kg) and histone injection (Sur+His; 45000 ± 10247 cells/mL; n=6). Summary data for the total protein leakage into the BALF at 4 hours after saline (control; 188 ± 19 μg/mL; n=5), histones (His; 45 mg/Kg; 1215 ± 186 μg/mL; n=9), or suramin (50 mg/Kg) and histone injection (Sur+His; 507 ± 66 μg/mL; n=5) and 24 hours after saline (control; 239 ± 21 μg/mL; n=5), histones (His; 45 mg/Kg; 901 ± 249 μg/mL; n=9), or suramin (50 mg/Kg) and histone injection (Sur+His; 225 ± 39 μg/mL; n=7). Data are expressed as mean ± SEM. Two-way ANOVA with Bonferroni's correction for multiple comparisons; $P<0.05$. A new biological replicate was used for each survival study experimental group, H&E staining (n=3 for each group), cell counts and total protein in BALF measurements.